PAPER

Generation of stacking faults in 4H-SiC epilayer induced by oxidation

Materials Research Express

RECEIVED
25 October 2017

REVISED
27 November 2017

ACCEPTED FOR PUBLICATION
8 December 2017

PUBLISHED
4 January 2018

PAPER

Generation of stacking faults in 4H-SiC epilayer induced by oxidation

Ryosuke Asafuji and Yasuto Hijikata

Division of Mathematics Electronics and Information Sciences, Graduate School of Science and Engineering, Saitama University, 255 Shimo-Okubo, Sakura-ku, Saitama-city, Saitama 338-8570, Japan

E-mail: yasuto@opt.ees.saitama-u.ac.jp

Keywords: 4H-SiC, oxidation, stacking fault, photoluminescence, line-/band-shaped fault

Abstract

Stacking faults (SFs) generated by thermal oxidation of a 4H-SiC epilayer were investigated using photoluminescence (PL) imaging/mapping and transmission electron microscopy (TEM). Line-shaped and band-shaped faults perpendicular to the off-cut direction in the epilayer were formed by thermal oxidation. In addition, the line-shaped faults increased and were stretched with the oxidation time. Triangular SFs were also formed under UV laser irradiation from both types of faults as starting points, and expanded along the basal plane toward the sample surface. The oxidation time dependence of the line-shaped fault density indicated that line-shaped faults are predominantly formed close to 1100 °C. The atomic structures of the line-shaped faults and triangular SFs were observed using cross-sectional TEM. Line-shaped faults were present at the epilayer/bulk interface with which double Shockley SFs stretch into the bulk layer. PL mapping results indicated that the band-shaped faults are probably intrinsic Frank-type SFs.

1. Introduction

Silicon carbide (SiC) semiconductors are studied actively for the development of low-loss, high-temperature, and high-frequency power devices, due to their superior physical properties [1]. However, stacking faults (SFs) and/or dislocations are easily incorporated in SiC epilayers [2–5], which may cause severe degradation of the SiC device performance [6–10]. SFs in SiC crystals have been reported to cause degradation of the breakdown field strength of Schottky barrier diodes (SBDs [9]) and the forward current of pin diodes [10]. Therefore, it is important to investigate the mechanism for the formation of SFs in the SiC epilayer. Thermal oxidation is often used in the fabrication of SiC devices because SiO_2 films grown by oxidation are utilized for metal-oxide-semiconductor junctions or as surface passivation films. However, it has been reported that thermal oxidation causes faults to form in the SiC crystal substrate. For example, Okojie *et al* reported that thermal oxidation produced multiple SFs with the 3C structure in a highly doped (10^{19} cm^{-3} order) 4H-SiC epilayer [11]. On the other hand, we have identified that line-shaped faults were formed perpendicular to the off-cut direction by thermal oxidation [12]. In addition, triangular SFs were formed by UV laser irradiation and expanded from the line-shaped faults. It is well known that oxidation-induced SFs (OSFs) are formed perpendicular to the Si substrate surface by the accumulation of Si interstitials emitted into the substrate during oxidation [13]. We presumed that the line-shaped faults are a type of OSF because the formation of line-shaped faults was specific to thermal oxidation, and the faults increased and were stretched with extension of the oxidation time [12]. In this study, we investigated the mechanism for the formation of line-shaped faults using photoluminescence (PL) imaging/mapping to reveal the identity of the line-shaped fault. Furthermore, transmission electron microscopy (TEM) was used to observe the atomic arrangement in the vicinity of line-shaped faults with triangular SFs.

2. Experimental procedure

An n-type 4H-SiC (0001) epilayer with a carrier concentration of 1×10^{16} cm^{-3}, 8° off-orientation towards the [11$\bar{2}$0] direction, and a thickness of 10 μm on an n-type bulk substrate with a carrier concentration in the order

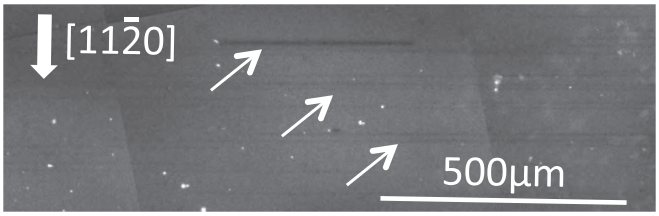

Figure 1. PL image of the line-shaped faults (BPF: 438 ± 12 nm). Thin arrows point to the line-shaped faults.

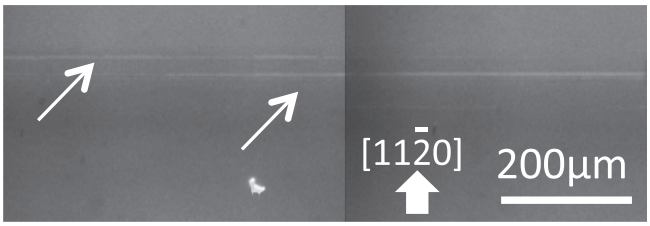

Figure 2. PL image of the line-shaped faults (BPF: 500 ± 12 nm). Thin arrows point to the line-shaped faults.

of 10^{19} cm^{-3} was used in this study. Thermal oxidation was conducted at temperatures of 1000 °C, 1100 °C, and 1200 °C in a dry oxygen flow of 1 slm. PL imaging was performed before and after each thermal oxidation step. A He–Cd laser ($\lambda = 325$ nm) with an irradiation power of 14 mW was used as the excitation source for PL imaging. PL images were captured with a cooled CCD camera through a band-pass filter (BPF: 438 ± 12 nm/ 500 ± 12 nm) at room temperature. PL mapping and spectroscopy measurements were performed using a confocal fluorescence microscope. The third harmonic of a YAG laser with a wavelength of 355 nm and an irradiation power of 10 mW was used as the excitation source. Spectra at each measurement point were recorded with a CCD diffraction grating spectrometer. UV laser irradiation was conducted using a diode-pumped solid-state laser with a wavelength of 266 nm and an irradiation power of 15 mW, or with the YAG laser.

TEM observation of the sample was performed after dry oxidation at 1100 °C for 32 h. TEM samples were sliced after forming protective films of carbon (C) and tungsten (W) on the surface. For the observation of SFs, the TEM sample was trimmed using a focused ion beam process followed by Ar milling.

3. Results and discussion

3.1. Observation of line-shaped faults

First of all, we attempted to confirm the formation of the line-shaped fault that was reported in [12]. According to the report from Miyano *et al* [12], the line-shaped fault is defined as a line-type fault that is observed by PL imaging with a 438 ± 12 nm BPF and is grown and stretched toward the [1$\bar{1}$00]/[$\bar{1}$100] as the oxide growth. Figure 1 shows a representative PL image including the line-shaped faults (solid arrows). This PL image was obtained through the 438 ± 12 nm BPF from the sample after oxidation at 1100 °C for 32 h. All the line-shaped faults were formed perpendicular to the off-cut direction. Figure 2 shows a PL image obtained with the 500 ± 12 nm BPF. PL from some of the line-shaped faults was observed in this wavelength range. Taking the emission wavelength range into account, this fault is presumably a band-shaped fault in the early stage of formation, which will be discussed later.

Figure 3 shows the oxidation time dependence of line-shaped fault densities at various oxidation temperatures. At 1100 °C, line-shaped faults started to form after 600 min of oxidation and their density increased with the oxidation time. In contrast, the line-shaped fault formed after 168 min oxidation at 1000 °C and only stretched until 2280 min. As for oxidation at 1200 °C, no line-shaped faults were formed, even after 4620 min. The formation of the line-shaped faults is thus significantly dependent on the oxidation temperature and is notably enhanced at around 1100 °C.

3.2. Observation of band-shaped faults

Apart from the line-shaped faults, band-shaped faults were also identified, as shown in figure 4. Figures 4(a)–(c) show PL images for samples oxidized at 1100 °C for 22 h, 32 h, and 32 h followed by Ar annealing for 1 h, respectively. The band-shaped faults were observed when the 500 ± 12 nm BPF was used for PL imaging, and these faults extended along the same direction as the line-shaped faults. The band-shaped faults appeared after

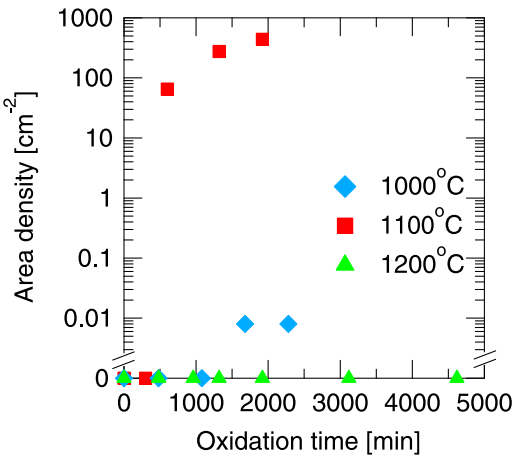

Figure 3. Line-shaped faults density as a function of oxidation time at various oxidation temperatures.

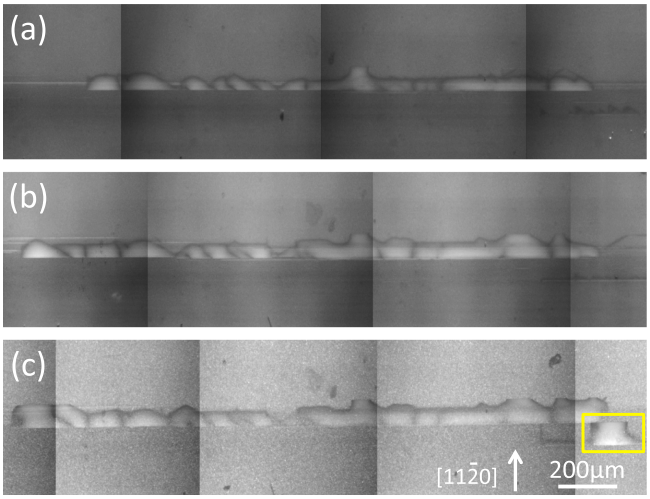

Figure 4. PL images for samples oxidized at 1100 °C for (a) 22 h, (b) 32 h, and (c) 32 h followed by Ar annealing for 1 h. Band-shaped fault formed by post-oxidation Ar annealing is indicated by a yellow box.

oxidation at 1100 °C for 22 h and were extended after oxidation for 32 h. Furthermore, after 1 h Ar annealing, the band-shaped fault was expanded more and a new band-shaped fault was formed at another line-shaped fault as a baseline (yellow box). Note that the direction [11$\bar{2}$0] was confirmed by x-ray diffraction measurement after the sample was prepared. Although the straight line of the band-shaped fault appears to be like a surface edge, it is the epilayer/bulk interface. In section 3.1, the emission wavelength of some of the line-shaped faults was stated to be in the range of 500 ± 12 nm, which is the same as that for band-shaped faults. In addition, triangle SFs were formed from the band-shaped faults as a starting point by laser irradiation during measurement (data not shown). As shown in the next section, this phenomenon was also observed for the line-shaped faults. These results suggest that the band-shaped faults originate from the line-shaped faults. In addition, the band-shaped fault was not shrunk by oxidation or annealing; therefore, it is considered to be a Frank-type SF [3]. On the other hand, band-shaped faults were not observed for oxidation at 1000 °C and 1200 °C.

3.3. UV laser irradiation of line-shaped faults

The impact of UV (355/266 nm) laser irradiation on the line-shaped faults was investigated. Figures 5(a) and (b) show PL images after laser irradiation at 355 nm and 266 nm, respectively. Laser irradiation at 355 nm and 266 nm induced the formation of triangle SFs, as observed through the 438 ± 12 nm and 500 ± 12 nm BPFs, respectively, and these triangular SFs were expanded from the line-shaped faults toward the sample surface (//[11$\bar{2}$0]) with an increase in the irradiation dose. Note that the direction [11$\bar{2}$0] shown in figure 5(b) was decided by x-ray diffraction measurement. These SFs are different from typical SFs often observed as in-grown SFs or electrical current-induced SFs when considering that the long side of the triangle faces not toward the

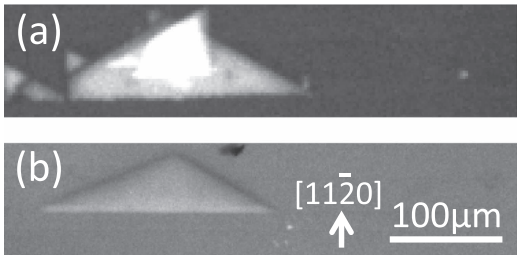

Figure 5. PL images observed through 438 ± 12 nm and 500 ± 12 nm BPFs after laser irradiation at (a) 355 nm and (b) 266 nm, respectively.

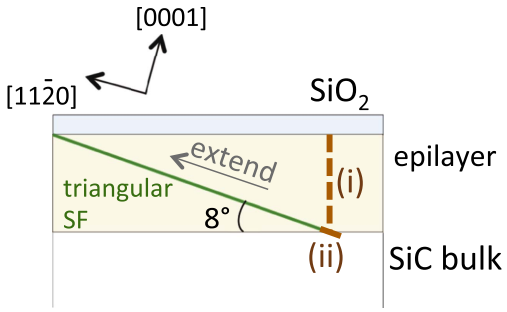

Figure 6. Schematic diagram of triangular SF and line-shaped fault.

surface side but toward the bulk layer side, and the SF extends from the epilayer/bulk interface to the surface. It can be considered that this difference has arisen because the SF induced by oxidation is formed by stress propagating from the oxidation interface. Namely, the stress propagates from the surface to the inside of substrate and the source of SF is located at the epilayer/bulk interface, both of which are opposite to typical SFs. Taking the emission wavelength into account, the triangle SFs induced by laser irradiation at 355 nm and 266 nm are a single Shockley SF (1SSF [4, 5, 14]) and a double Shockley SF (2SSF [15, 16]), respectively. The heights of the triangular SFs were stretched toward the [11$\bar{2}$0] direction and, in turn, the extension of the triangular SFs stopped when their height reached the length that corresponds to the thickness of the epilayer. The triangular SFs then deformed to trapezoids and expanded toward the [1 $\bar{1}$ 00] or [$\bar{1}$ 100] directions. These results reveal that triangular SFs are formed inside the epilayer and expand from the epilayer/bulk interface to the sample surface, as illustrated in figure 6. The triangle SF induced by laser irradiation is generated from a line-shaped fault as a baseline; therefore, it is inferred that the line-shaped fault is a type of SF. These results suggest that the structure of the line-shaped fault is similar to that of an OSF that extends from the sample surface to the epi–bulk interface (shown by a brown dashed line in figure 6(i)), or is similar to the interface dislocation present at the epi–bulk interface [17] (brown solid line in figure 6(ii)).

3.4. TEM observation

Figures 7(a) and (b) show a PL image with the position of the TEM observation and cross-sectional TEM image near the sample surface, respectively. In figure 7(a), the yellow area denotes the trimming area for TEM observation and the thin arrow is the observation direction. Figure 7(b) shows that no contrast considered to be a line-shaped fault or a triangular SF was observed. The results indicate that both line-shaped faults and triangular SFs are not present near the surface. Therefore, it is concluded that the structural model shown in figure 6(i) can be excluded and the line-shaped fault specific to SiC oxidation is not a type of OSF formed during Si oxidation.

Figures 8(a)–(c) show a PL image with the position of TEM observation, cross-sectional TEM image around the epilayer/bulk interface, and a magnified image of 8(b), respectively. No contrast in figures 8(b) and (c) considered to be a line-shaped fault was observed, but two contrasts, which appeared to be SFs, were observed. Although one of these propagated across the epilayer/bulk interface from the bulk layer, the other stopped near the epi/bulk interface. Figures 9(a) and (b) show magnified images of Points A and B shown in figure 8(c), respectively. The stacking sequence at Point A (near the edge) was found to be a 1SSF and that at Point B (away from the edge) was a 2SSF. Therefore, most of the triangular SFs are 2SSFs, but in the propagating head the triangular SFs are 1SSFs. In figure 9(a), a SF looking like Frank-type SF can be seen. As will be discussed later, this may be the line-shaped fault.

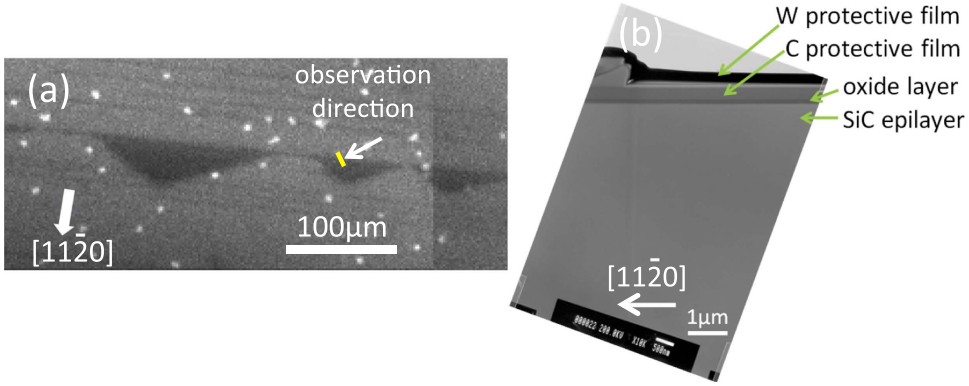

Figure 7. Cross-sectional TEM image around the sample surface: (a) PL image showing the TEM observation point and (b) TEM image.

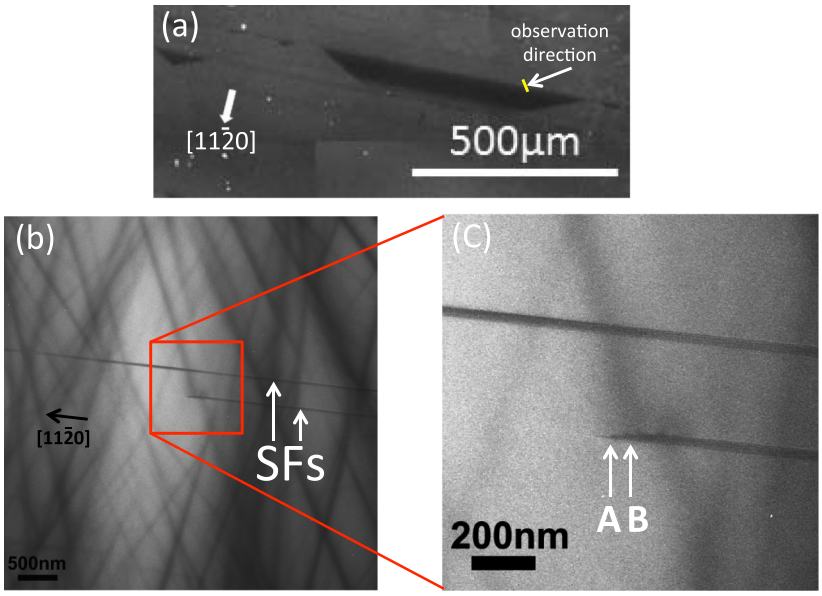

Figure 8. Cross-sectional TEM image around the epi/bulk interface: (a) PL image showing the TEM observation point, (b) TEM image, and (c) magnified image of (b); Points A and B denote the observation points for figures 9 (a) and (b), respectively.

The TEM images in figures 8(b) and (c) indicate that the 2SSFs extended to the bulk layer. On the other hand, figure 8(a) does not show the SF in the bulk layer by PL imaging. It is probable that non-radiative recombination centers are dominant in the bulk layer, which results in PL from the SF in the bulk layer disappearing.

3.5. PL mapping and spectroscopic measurements

PL mapping and spectroscopy measurements were performed for the area including line-shaped faults and a band-shaped fault. Note that, as discussed in section 3.3, there is no formation of 2SSFs during PL measurement in the case of 355 nm laser excitation. Figure 10 shows a PL image with the PL mapping area indicated by a yellow box (500 ± 12 nm BPF), PL maps filtered with 4H-SiC band-edge emission, 2SSF emission, and 488 ± 5 nm BPF. Figure 10(a) shows that there are few line-shaped faults on the left-side from the band-shaped fault, and many of them on the right-side. The PL maps show that the band-edge emission becomes strong where there are few line-shaped faults, whereas the 2SSF emission becomes strong where there are many line-shaped faults. Therefore, the 2SSF is a by-product of the line-shaped fault.

Figure 10(d) clearly shows the contrast of the band-shaped fault. Figure 11 shows PL spectra taken at Points A–C shown in figure 10(d). Differential spectra, i.e. the spectrum measured at Point B minus that at Point A (B – A) and C – A, are also shown in figure 11. Figure 10(d) and the differential spectrum (B – A) in figure 11 indicate that the emission wavelength of the band-shaped fault is around 485 nm, which is considered to be an emission from an intrinsic Frank-type SF [3] or triple Shockley SF (3SSF) [4, 5]. The band-shaped fault was not

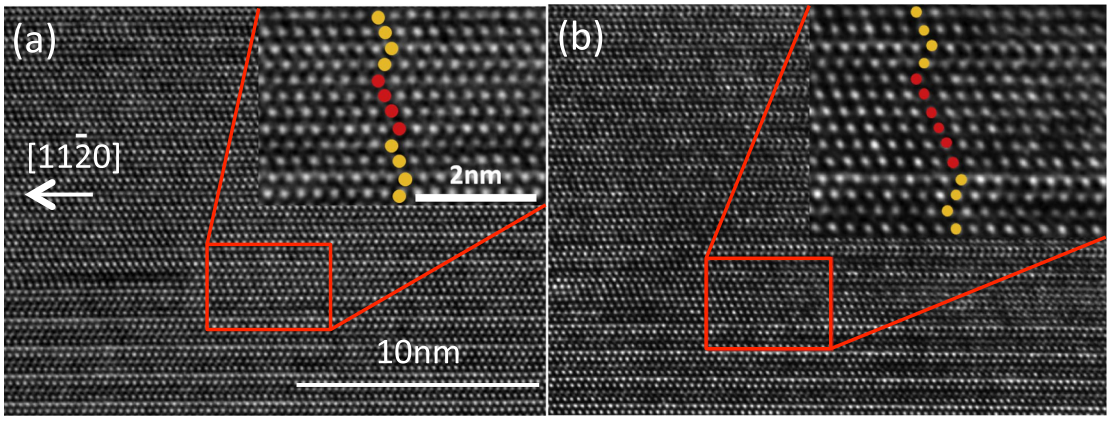

Figure 9. Atomic arrangement of the SF at (a) Points A and (b) B indicated in figure 8(b).

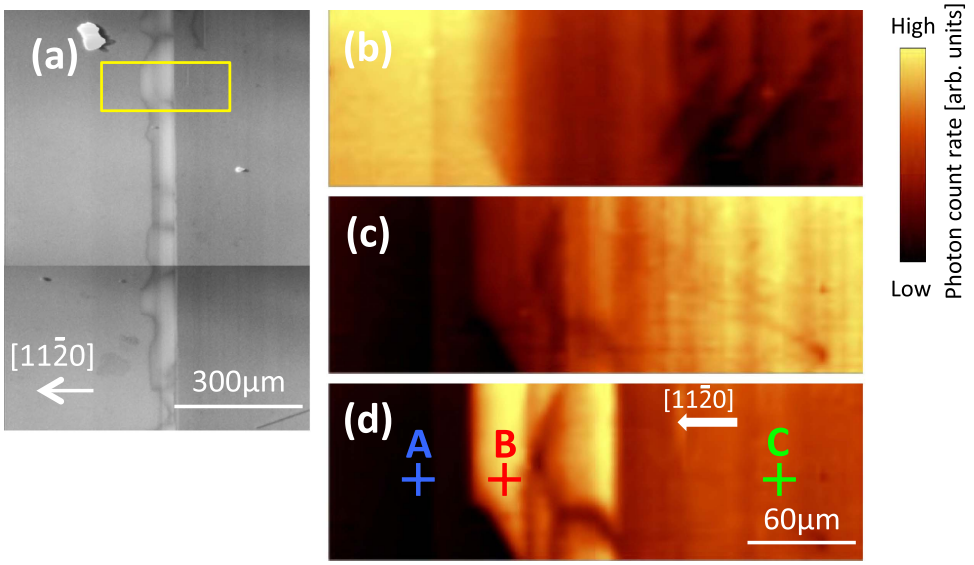

Figure 10. (a) PL image with the PL mapping area indicated by a yellow box (500 ± 12 nm BPF) and PL maps filtered with (b) 4H-SiC band-edge emission (390 ± 5 nm BPF), (c) 2SSF emission (500 ± 5 nm BPF), and (d) 488 ± 5 nm BPF; Points A–C denote the measured points for the spectra in figure 11.

shrunk by annealing, as revealed in section 3.2, which infers that the band-shaped fault is an intrinsic Frank-type SF. Careful inspection of the differential spectra reveals that the area dense with 2SSFs (i.e. dense with line-shaped faults) does not contain band-shaped faults, whereas the low density area of 2SSFs contains band-shaped faults. Therefore, we consider that the band-shaped fault is a fault extended from the line-shaped fault as its origin. Also discussed in section 3.2, there are many common characteristics between band-shaped and line-shaped faults, such as the effect of UV laser irradiation. Therefore, it is presumable that the line-shaped fault is also an intrinsic Frank-type SF. Comparison of figures 10(a) with (c) reveals the PL map has emission from 2SSFs in the bulk layer in the vicinity of the line-shaped faults, whereas the PL image did not show the emission well. This discrepancy is probably due to the confocal optical system that enhances the PL detection of line-shaped faults because of its higher surface sensitivity.

3.6. Configuration of faults

Figure 12 shows a schematic illustration of the faults observed in this study. According to TEM observations, line-shaped faults are located at the epi–bulk interface, from which 2SSFs are extended toward the bulk layer by oxidation (figure 12(i)). When the line-shaped fault is irradiated with UV irradiation, 1SSF/2SSF is formed and extended toward the sample surface with an increase of the irradiation dose (figure 12(ii)). As shown in figure 2, some of the line-shaped faults are converted to band-shaped faults (figure 12(iii)), and as shown by figure 4,

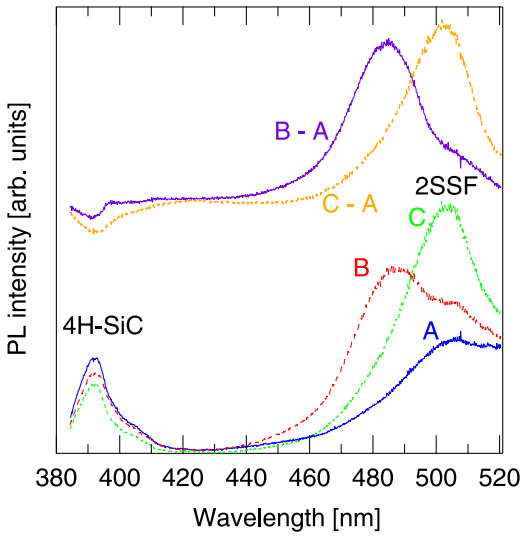

Figure 11. PL spectra measured at the Points A–C shown in figure 10(d). Differential spectra (B–A) and (C–A) are also shown.

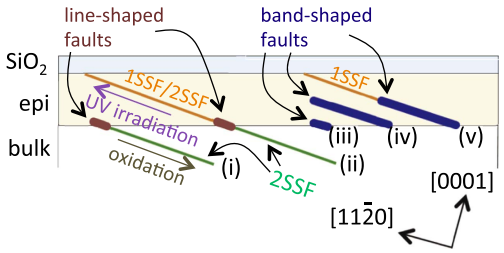

Figure 12. Schematic diagram of the faults observed in this study; (i) line-shaped fault with a 2SSF in the bulk layer, (ii) line-shaped fault with a 1SSF/2SSF in the epilayer and a 2SSF in the bulk layer, (iii)/(iv) (an extended) band-shaped fault, (v) a band-shaped fault with a 1SSF in the epilayer.

some of them are further expanded toward the surface (figure 12(iv)). A band-shaped fault with 1SSF induced by 355 nm laser irradiation was also identified, as illustrated in figure 12(v).

At the moment the formation mechanisms of the line-shaped and the band-shaped fault are unclear, but the stress at the oxide–SiC interface during oxidation may involve the formation of the faults. Namely, the SiC epilayer receives an intense lattice expansion because the density of SiO_2 is twice lower than that of SiC [18] and, as a result of SiC robustness, a strain is brought about at the interface and propagates toward the SiC epilayer. According to the report from Goto and Hijikata [19], since the Si atom emission rate decreases with increasing the oxidation temperature, it is expected that the stress to the SiC layer becomes smaller at the higher temperature. On the other hand, the condensing of defect and the formation of the line-shaped faults should be enhanced at higher temperature and, thus, the formation rate of the line-shaped fault is considered to have a maximum at some oxidation temperature, which is consistent with the temperature dependence of the formation rate shown in section 3.1.

Another possibility of the cause for the line-/band-shaped faults formation is that a 2SSF is grown from the backside of the substrate (i.e. [000 $\bar{1}$] C-face) and the 2SSFs are transformed to the line-shaped faults (in turn, the band-shaped faults) at the epilayer–bulk interface. Since the oxidation rate of C-face is much faster than that of Si-face, the generation of Si interstitials and the absorption of them into the growing oxide might be comparable, resulting in the maximum of the temperature dependence of the density of the line-shaped faults. PL imaging for both-side polished substrate might solve this issue.

4. Summary

The formation of SFs generated by thermal oxidation was observed using PL imaging/mapping and TEM. Line-shaped and band-shaped faults were expanded with the oxidation time. UV laser irradiation at 355 nm or

266 nm of these faults formed 1SSFs or 2SSFs, respectively, from line-/band-shaped faults as starting points along the [11$\bar{2}$0] direction. The oxidation time dependence of the line-shaped fault density indicated that the formation of line-shaped faults is significantly enhanced at around 1100 °C. TEM observations indicated that line-shaped faults are not present at the surface of the substrate but at the epilayer/bulk interface, and they combine with 2SSFs and propagate into the bulk layer from line-shaped faults as a starting point. The origin of the line-shaped faults, as well as that of the band-shaped faults, is probably intrinsic Frank-type SFs because of their emission wavelength and their behavior under the effect of annealing.

Acknowledgments

This work was supported in part by a Grant-in-Aid for Scientific Research (#15H03967) from the Japan Society for the Promotion of Science (JSPS).

ORCID iDs

Yasuto Hijikata https://orcid.org/0000-0002-6314-0401

References

[1] Matsunami H and Kimoto T 1997 *Mater. Sci. Eng.* R **20** 125
[2] Tsuchida H, Kamata I and Nagano M 2008 *J. Cryst. Growth* **310** 757
[3] Kamata I, Zhang X and Tsuchida H 2010 *Appl. Phys. Lett.* **97** 172107
[4] Feng G, Suda J and Kimoto T 2008 *Appl. Phys. Lett.* **92** 221906
[5] Feng G, Suda J and Kimoto T 2009 *Appl. Phys. Lett.* **94** 091910
[6] Lendenmann H, Dahlquist F, Johansson N, Soderholm R, Nilsson P A, Bergman J P and Skytt P 2001 *Mater. Sci. Forum* **353** 727
[7] Lendenmann H, Dahlquist F, Bergman J P, Bleichner H and Hallin C 2002 *Mater. Sci. Forum* **389** 1259
[8] Liu J Q, Skowronski M, Hallin C, Soderholm R and Lendenmann H 2002 *Appl. Phys. Lett.* **80** 749
[9] Fujiwara H, Kimoto T, Tojo T and Matsunami H 2005 *Appl. Phys. Lett.* **87** 051912
[10] Nakayama K, Sugawara Y, Tsuchida H, Kimura C and Aoki H 2011 *Japan. J. Appl. Phys.* **50** 04DF04
[11] Okojie R S, Xhang M, Pirouz P, Tumakha S, Jessen G and Brillson L J 2001 *Appl. Phys. Lett.* **79** 3056
[12] Miyano Y, Asafuji R, Yagi S, Hijikata Y and Yaguchi H 2015 *AIP Adv.* **5** 127116
[13] Dunham S T and Plummer J D 1986 *J. Appl. Phys.* **59** 2551
[14] Hassan J and Bergman J P 2010 *Mater. Sci. Forum* **645** 327
[15] Liu J Q, Chung H J, Kuhr T, Li Q and Skowronski M 2002 *Appl. Phys. Lett.* **80** 2111
[16] Chung H J, Liu J Q and Skowronski M 2002 *Appl. Phys. Lett.* **81** 3759
[17] Matsuhata H, Yamaguchi H, Nagai I, Ohno T, Kosugi R and Kinoshita A 2009 *Mater. Sci. Forum* **600–603** 309
[18] Hijikata Y, Yaguchi H and Yoshida S 2009 *Appl. Phys. Express* **2** 021203
[19] Goto D and Hijikata Y 2016 *J. Phys. D: Appl. Phys.* **49** 225103